Switching Molecular Conformation with the Torque on a Single Magnetic Moment

Aram Kostanyan,[1,*] Rasmus Westerström,[1,2] Yang Zhang,[3] David Kunhardt,[3] Roland Stania,[1,†] Bernd Büchner,[3] Alexey A. Popov,[3] and Thomas Greber[1,‡]

[1]*Physik-Institut, Universität Zürich, Winterthurerstrasse 190, CH-8057 Zürich, Switzerland*

[2]*Division of Synchrotron Radiation Research, Institute of Physics, University of Lund, SE-221 00 Lund, Sweden*

[3]*Leibniz Institute of Solid State and Materials Research, Dresden, D-01069 Dresden, Germany*

(Received 23 June 2017; revised manuscript received 26 October 2017; published 5 December 2017)

For the endohedral fullerene molecule $HoLu_2N@C_{80}$, it is shown that the endohedral $HoLu_2N$ unit may be oriented in a magnetic field. The Ho magnetic moment is fixed in the strong ligand field and aligns along the holmium-nitrogen axis. The torque of a magnetic field on the Ho magnetic moment leads to a hopping bias of the endohedral unit inclining to an orientation parallel to the externally applied field. This endohedral cluster distribution remains frozen below the onset of thermally induced rotation of the endohedral units. We derive an analytical statistical model for the description of the effect that scales below 7 T with the square of the external field strength, and that allows us to resolve the freezing temperature of the endohedral hopping motion. The freezing temperature is around 55 K and depends on the cooling rate, which in turn determines an activation energy for the hopping motion of 185 meV and a prefactor of 1.8×10^{14} s^{-1}. For $TbSc_2N@C_{80}$ we find the same behavior with a 3.5% higher freezing temperature.

DOI: 10.1103/PhysRevLett.119.237202

The needle of a compass easily orients in a magnetic field because the torque scales with the sum of the electronic moments that are frozen in the lattice of the ferromagnetic needle. Still, magnetic moments of single atoms may be oriented and if the torque is transferred to the surrounding of the moment, as it is a molecule or a crystal, macroscopic rotation may result as well. In order to search for this orientation effect in the single atom limit, the ratio X between Zeeman energy and thermal energies $\mu B/k_B T$ has to be considered. For an atomic moment μ of 10 μ_B and a magnetic field of 1 T, X is larger than one below 7 K. This scaling argument limits expectations to see B field induced rotation due to a single paramagnetic atom. For example, the alignment of rare-earth-containing liquid crystals in B fields of about 1 T and above room temperature [1] must be a cooperative phenomenon, where more than one moment is involved. For isolated paramagnetic atoms in molecules, so far, no changes of the molecular conformation upon application of a magnetic field have been demonstrated. Here we report the alignment of the endohedral unit of $HoLu_2N@C_{80}$ [Fig. 1(a)] in an externally applied magnetic field. With careful field and temperature dependent magnetization measurements, a single magnetic moment effect on the molecular conformation is shown. The endohedral unit is subject to thermally activated hop rotation between equivalent low energy conformations [2,3], way below the freezing temperature of the carbon cages in a solid, which is 250 K for the case of solid C_{60} [4]. The magnetic field exerts a torque on the Ho^{3+} ion that is transferred to the endohedral unit because of the magnetic anisotropy, i.e., the alignment of the Ho magnetic moment in a strong ligand field, that is the base of single molecule [5,6] and single atom magnetism [7,8].

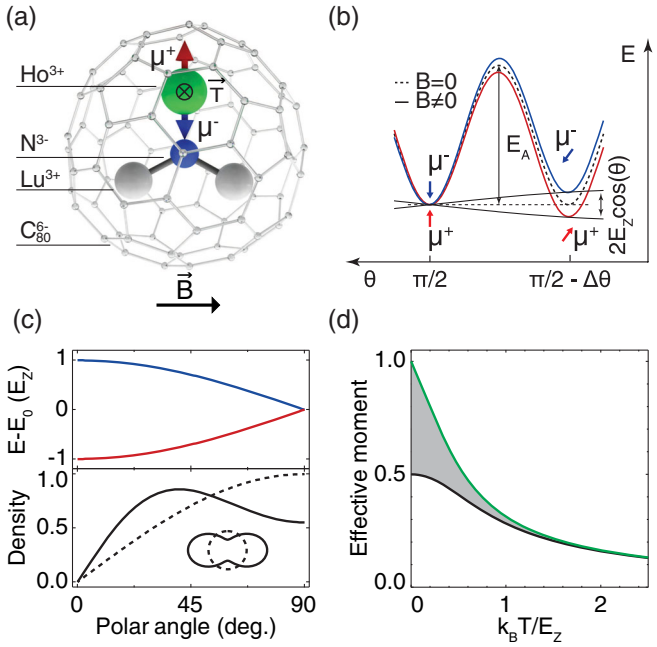

FIG. 1. (a) Ball-and-stick model of $HoLu_2N@C_{80}$. A $\vec{B}$ field exerts a torque $\vec{T}$ on the Ho magnetic moment $\vec{\mu}$. (b) The energy barrier E_A separates preferred orientations separated by $\Delta\theta$, while the Zeeman energy imposes a bias for magnetic moments parallel to the $\vec{B}$ field. (c) (top) Zeeman splitting and (bottom) angular density distribution dependence on the polar angle. The equilibrium angular density distribution for $E_Z = 0$ (dashed line) and $k_B T/E_Z = 1/2$ (solid line) are shown. The inset is the polar diagram of the two distributions. (d) Effective magnetic moment in thermal equilibrium vs $k_B T/E_Z$ for freely rotating endohedral units (green) and for frozen, isotropically distributed magnetic moments (black). The magnetization of in-field cooling should lie within the green and the black curves in the shaded area.

$HoLu_2N@C_{80}$ endofullerenes were produced by arc-discharge synthesis using corresponding metal oxides and guanidine thiocyanate as the nitrogen source. The resultant soot was preextracted with acetone and further Soxhlet-extracted with CS_2. The separation of different fullerenes was performed by two-step high pressure liquid chromatography. The complete separation of $HoLu_2N@C_{80} - I_h$ from $Lu_3N@C_{80} - I_h$, I_h being the most abundant isomer with icosahedral symmetry, was not possible without significant loss of material; thus, the sample used for this Letter contained 20% of diamagnetic $Lu_3N@C_{80} - I_h$ [2]. Hereafter we will omit the isometric label I_h.

The magnetization measurements were performed in a Quantum Design MPMS3 Vibrating Sample Magnetometer (VSM). The sample is drop cast from toluene solution [9] that results in a black powder, and from the saturation magnetization we calculate a mass of 0.5 mg $HoLu_2N@C_{80}$. A temperature independent diamagnetic background of -3×10^{-8} Am^2/T was inferred from the low temperature magnetization data between 5 and 7 T.

Figure 1(a) shows the model of $HoLu_2N@C_{80}$. The endohedral unit consists of a triangle with 3 trivalent rare earth ions on its vertices, in the present case two diamagnetic Lu^{3+} and one paramagnetic Ho^{3+} ion. In the center of the triangle sits a nitrogen 3^- ion that lifts the 17-fold degeneracy of the isotropic Ho $^5I_8$ Hund ground state. As for $HoSc_2N@C_{80}$ [6], the ground state assumes $J_z = \pm 8$ with a large nominal magnetic moment $\mu = 10\ \mu_B$, where the quantization axis aligns along the N-Ho axis. Point charge model calculations of the ligand field splittings indicate an energy difference $\Delta E/k_B$ of 300 K between the first excited state $J_z = \pm 7$ and the ground state $J_z = \pm 8$. Therefore, in the temperature range of our experiment, the magnetism is described with a single pseudospin $J_z = \pm 8$ [2]. Such axial anisotropy is found as well for Dy [9,10] and for Tb [11]. A magnetic field $\vec{B}$ exerts a torque $\vec{T} = \vec{\mu} \times \vec{B}$ on the Ho atom. The anisotropy of the ligand field, however, hinders the Ho magnetic moment from freely following the magnetic field, and the torque is transferred to the N-Ho bond that acts as a lever for the torque on the endohedral unit, and the carbon cage. The free rotation of the endohedral units and the molecules is hindered by the nonisotropic carbon cages that impose preferred endohedral orientations [2].

For the given magnetic moment density, magnetic dipole interaction between different molecules may be neglected above temperatures of 1 K [12].

A priori it cannot be decided on whether the endohedral units rotate with the crystal, with the cage, or within the cage. The reproducibility of the experiment excludes macroscopic changes in the sample, while the length of the lever, the lower coordination, and the activation energy E_A that we determine rather favor a picture where the endohedral unit moves inside the cage in an otherwise frozen sample. This is also in line with the higher temperatures at which the onset of molecular rotation in solid C_{60} was observed [4]. Based on molecular dynamics simulations the motion of the endohedral unit is a thermally activated hopping between symmetrically equivalent sites, i.e., conformations, in the C_{80} cage [2]. This picture is also corroborated by nuclear magnetic resonance experiments [13,14]. In Fig. 1(b) a simplified, one-dimensional scheme of a potential energy landscape is shown, where two minima are separated by E_A. The first minimum corresponds to conformations with the magnetic moment perpendicular to the magnetic field ($\theta = \pi/2$), while the second minimum is separated by the angle between two neighboring conformations $\Delta\theta$. In this second minimum, the two magnetic moments are split by a Zeeman energy of $\vec{\mu} \cdot \vec{B} = 2E_Z \sin(\Delta\theta)$, where $E_Z = \mu B$. At low temperatures the two states are not populated equally and the B field imposes a drag toward small polar angles, i.e., causes an orientation of the endohedral units. If, however, the activation energy $E_A \gg k_B T$, the system may not assume thermal equilibrium in the accessible time frame. In the top panel of Fig. 1(c) the polar angle dependence of the Zeeman energy is depicted for the two zero field ground states $\pm J_z$ with the energy scale E_Z. In the lower panel, the density of the moments as a function of the polar angle is shown for the isotropic distribution ($k_B T \gg E_Z$) and for $k_B T/E_Z = 1/2$. The statistical mechanics problem of the determination of the density and the corresponding average magnetic moment may be solved analytically. In Fig. 1(d) the isotropic and the equilibrium magnetizations are shown as a function of temperature. For the green equilibrium curve, the moments will orient collinear to the magnetic field at zero Kelvin. On the other hand, the saturation magnetization for the isotropic distribution of the moments reaches only half of the collinear case [15]. Therefore, we expect a magnetization between the equilibrium and the isotropic case [gray area in Fig. 1(d)], depending on whether the sample is cooled in zero field or in an externally applied magnetic field.

Figure 2(a) shows the effect of field induced orientation of Ho magnetic moments as expressed by the magnetic moment m of the sample. The black trace is the zero-field cooled magnetic moment m_z during warm-up in an applied field $\mu_0 H = 7$ T. The red trace, on the other hand, is the magnetic moment m_i as observed when the sample is cooled and warmed-up in an externally applied field ($\mu_0 H = 7$ T). Clearly, below a certain temperature, the zero-field cooled sample displays a lower magnetization than the in-field cooled sample. The effect depends on the applied magnetic field, and as we see later on the cool-down and warm-up rate $\pm\beta$ that was set for the data in Fig. 2 to $\pm\beta = 5 \times 10^{-2}$ K/s. Figure 2(b) shows the ratio of the magnetic moment between in-field and zero-field cooled sample m_i/m_z for different external magnetic fields. Above about 60 K the ratio m_i/m_z is one. Below this characteristic temperature, the hopping rates of the endohedral units drop, such that the equilibrium magnetization for the given temperature may not be obtained during the

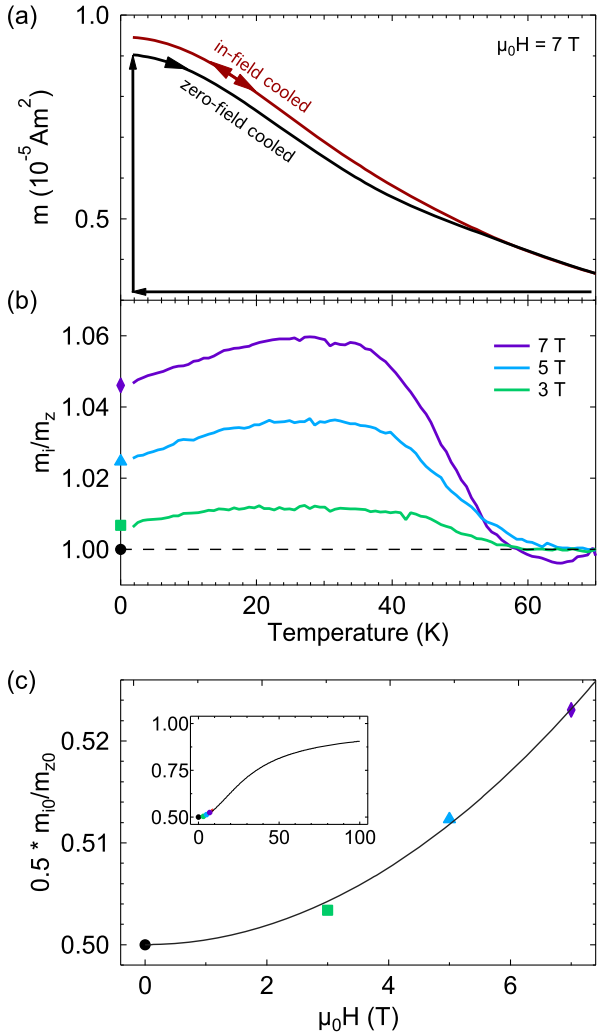

FIG. 2. (a) Temperature dependence of the magnetic moment m for zero-field cooled (black) and in-field cooled (red) $HoLu_2N@C_{80}$. (b) Ratio of the magnetic moment for in-field and zero-field cooled m_i/m_z for different externally applied magnetic fields (7 T, 5 T, 3 T). (c) $m_{i0}/m_{z0}/2$ extrapolated to 0 K. From the curvature of the parabola the Zeeman energy:k_BT_F ratio is inferred. Inset: Prediction for higher magnetic fields. Heating and cooling rate $\pm\beta = 5 \times 10^{-2}$ K/s K/s.

duration of the experiment. In the following, we will call this temperature the equilibrium freezing temperature T_F, at which the angular density distribution of the magnetic moments freezes. The zero Kelvin extrapolation $(m_i/m_z)_{T=0}$ increases with the externally applied field in a nonlinear fashion [see Fig. 2(c)]. For fields up to 7 T, we get a parabolic effect. Qualitatively, this can be understood by the effective magnetic torque, which is proportional to the external field and the magnetization that is, near zero, as well proportional to the external field. Using the second term $\propto B^2$ of the series expansion of the model in Fig. 1 $(m_i/2m_z)_{T=0}(B) = 1/2 + (aB)^2/24$ with $a = X_F/B = \mu/k_BT_F$. The experimental value of $a = (107 \pm 1) \times 10^{-3}$ T^{-1}. If we use the full analytical expression for the determination of a we get $(108.9 \pm 0.2) \times 10^{-3}$ T^{-1}. As it is shown in the inset of Fig. 2(c) the theory also predicts the orientation effect for large fields, where the effect flattens and approaches saturation.

If we want to determine T_F, we have to know the magnetic moment μ of the Ho atom. This can be obtained conveniently from the magnetization curves of zero-field cooled samples, as it was demonstrated for other noncollinear single-ion magnets [6,10,11]. The magnetization data in Fig. 3 were recorded at 1.8 K, well below the freezing temperature. If we apply a simultaneous fit to both magnetization curves in Fig. 3, where the number of molecules N and the magnetic moment μ have to assume the same value, and where we allow for the in-field cooled sample a freezing temperature T_F, we get $N = (2.02 \pm 0.005) \times 10^{17}$, $\mu = 9.55 \pm 0.02\ \mu_B$ and $T_F = 52.3 \pm 0.3$ K for $\beta = 5 \times 10^{-4}$ K/s. From data of a $TbSc_2N@C_{80}$ sample [16], we get $\mu = 9 \pm 0.02\ \mu_B$ and $T_F = 60.3 \pm 0.3$ K for $\beta = 5 \times 10^{-2}$ K/s. The noniso-tropic angular distribution of the magnetic moments for the in-field cooled sample corresponds to the equilibrium distribution at T_F and is responsible for the excess magnetization. Considering that the freezing temperature depends on β (see below) this is in perfect agreement (better than 3%) with the parameter a from the data in Fig. 2. Furthermore, the difference curve between m_i and m_z indicates that the difference between the in field and zero field is not explained by a simple scaling and it is seen that the conformational change model with a field dependent freezing temperature describes the data very well.

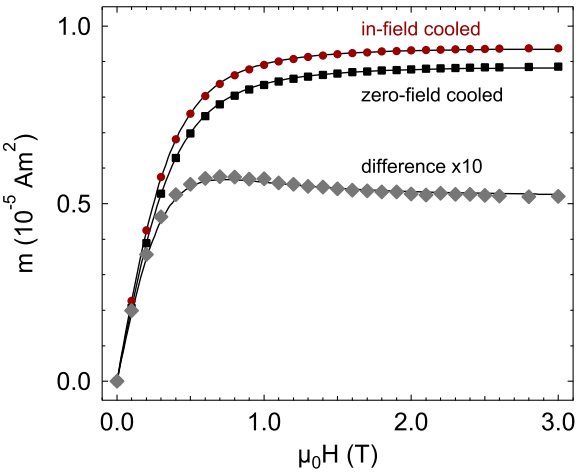

FIG. 3. Magnetization m vs externally applied magnetic field $\mu_0 H$ of $HoLu_2N@C_{80}$ at 1.8 K (raw data). Both zero-field (black squares) and in-field 7 T (red circles) cooled data were fitted (solid lines) simultaneously with a model of isotropically (randomly) oriented Ho magnetic moment and an equilibrium distribution with a freezing temperature T_F. The fits yield 9.55 μ_B for the Ho magnetic moment and a T_F of 52.3 K for $B = 7$ T and $\beta = 5 \times 10^{-4}$ K/s. Grey diamonds are the difference between zero-field and in-field cooled. The solid line is the difference of the corresponding fits.

In order to determine the activation energy E_A [see Fig. 1(b)] and the attempt frequency ν for the endohedral hop rotation, temperature sweep-rate dependent measurements were performed. Figure 4(a) shows the in-field and zero-field cooled ratio m_i/m_z for three different temperature sweep rates β between 5×10^{-4} K/s and 5×10^{-2} K/s. As expected, for small β's the endohedral unit has more time to adopt equilibrium during in-field cooldown, resulting in smaller T_F's as shown in Fig. 4(b), and larger endohedral orientation. The T_F's are determined from magnetization curves at 1.8 K for corresponding β's as described above.

E_A and ν are obtained from a first order kinetics model. In this model, we assume that during a time interval Δt the equilibrium is approached exponentially:

$$m(t + \Delta t) = m(t) + \Delta m_E[1 - \exp(-\Delta t/\tau)], \quad (1)$$

where $\Delta m_E = m_E(t + \Delta t) - m(t)$ is the deviation of the magnetization $m(t)$ at time t from the equilibrium magnetization m_E. The time constant τ is the average time between two hops and is described by a single barrier E_A. It has the form $\tau = (\nu \exp(-E_A/k_B T))^{-1}$, where ν is the attempt frequency and k_B is the Boltzmann constant. The best fit to the $T_F(\beta)$ data yields a barrier $E_A/k_B = (2145 \pm 20)$ K and $\nu = 1.8 \times 10^{14\pm0.15}$ s^{-1} where the confidence intervals are strongly correlated and taken at levels 10% above the χ^2 minimum between experiment and theory. The ratio between E_A and E_Z at 7 T is 47 which rationalizes the relatively high freezing temperatures.

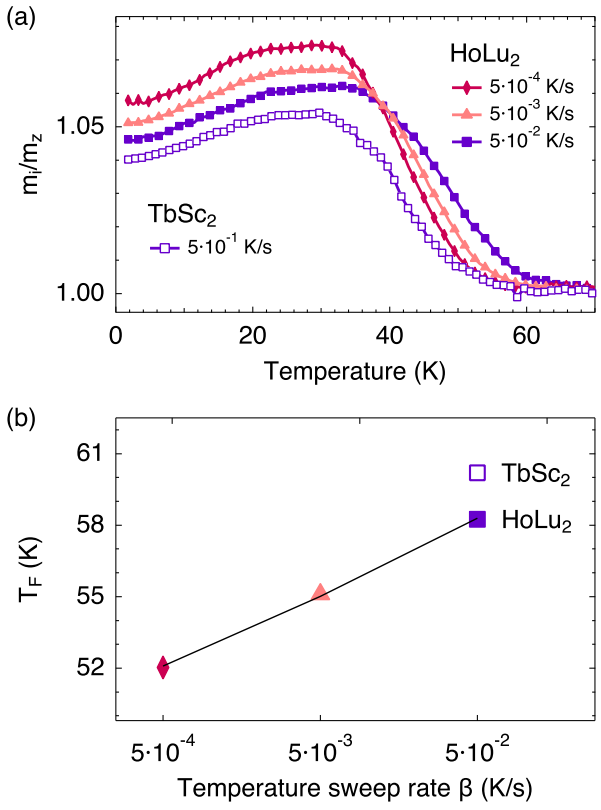

FIG. 4. (a) Ratio of magnetic moment for in-field and zero-field cooled m_i/m_z at different temperature sweep rates β for $HoLu_2$ (full symbols) and $TbSc_2$ (open symbols). (b) Freezing temperatures $T_F(\beta)$ [with corresponding symbols and colors from (a)] determined from fits of magnetization curves of the in-field cooled samples. The solid line is the best fit of first order kinetics for $HoLu_2$—with a barrier height $E_A/k_B = (2145 \pm 20)$ K and an attempt frequency $\nu = 1.8 \times 10^{14\pm0.15}$ s^{-1}.

The activation energy for the onset of endohedral rotation in C_{80} for $HoLu_2N$ (185 meV) compares well with Lu_3N (186 meV) as obtained from NMR [17], and studies for Sc_3N (78–150 meV) [3] This suggests an increase of E_A with the size of the endohedral cluster. The prefactor ν that is needed as well for a complete kinetic description is larger than the highest molecular vibration frequencies. This is not an inconsistency, large kinetic prefactors up to 10^{19} s^{-1} were, e.g., observed in desorption of alkane molecules on surfaces [18–20]. This may be an indication, that the one-dimensional two level picture as sketched in Fig. 1(b) is too simple. Rather, the large ν hints to the many degrees of freedom that are involved in the hopping of endohedral units in C_{80} [2]. The extracted kinetic parameters will allow the test of temperature dependent molecular dynamics simulations, and the study of steric effects due to different rare earth ion sizes. For example, the difference in freezing temperature between $HoLu_2$ and $TbSc_2$ in Fig. 4 indicates—under the assumption of the same prefactor—a 3.5% higher activation energy for the Tb compound. The kinetic parameters are also needed if the orientation effect shall be enhanced by high magnetic field pulses, as well as if the effect shall be applied for the orientation of the easy axis in endohedral single molecule magnets.

In conclusion, we have shown that endohedral units like $HoLu_2N$ or $TbSc_2N$ may be rotated inside C_{80} molecules by the application of magnetic fields. The Zeeman energy enables the rotation and its measurement of the effect in the magnetization. The ratio X_F between the Zeeman energy and thermal energies at freezing controls the degree of orientation, where T_F is governed by a characteristic time τ that describes the equilibration time. The presented conformational change model may be applied to other endohedral molecules containing a magnetic moment, and the corresponding activation energies will provide insight into the relation between the size of the endohedral cluster and its binding.

We gratefully acknowledge financial support from the Swiss National Science Foundation (SNF Projects No. 206021_150784, No. 200021L_147201, and No. 200020_153312), the European Research Council (ERC) under the European Union's Horizon 2020 research and innovation programme (Grant No. 648295 "GraM3") and the Swedish Research Council (Grant No. 2015-00455) and Sklodowska Curie Actions co-founding Project No. INCA 600398.

*Corresponding author.
aram@physik.uzh.ch
†Center for Artificial Low Dimensional Electronic Systems, Institute for Basic Science (IBS), Pohang, Republic of Korea.
‡greber@physik.uzh.ch

[1] K. Binnemans, Y. G. Galyametdinov, R. Van Deun, D. W. Bruce, S. R. Collinson, A. P. Polishchuk, I. Bikchantaev, W. Haase, A. V. Prosvirin, L. Tinchurina, I. Litvinov, A. Gubajdullin, A. Rakhmatullin, K. Uytterhoeven, and L. Van Meervelt, Rare-earth-containing magnetic liquid crystals, J. Am. Chem. Soc. **122**, 4335 (2000).

[2] Y. Zhang, D. Krylov, S. Schiemenz, M. Rosenkranz, R. Westerström, J. Dreiser, T. Greber, B. Büchner, and A. Popov, Cluster-size dependent internal dynamics and magnetic anisotropy of Ho ions in $HoM_2N@C_{80}$ and $Ho_2MN@C_{80}$ families (M = Sc, Lu, Y), Nanoscale **6**, 11431 (2014).

[3] T. Huang, J. Zhao, M. Feng, A. A. Popov, S. Yang, L. Dunsch, and H. Petek, A multi-state single-molecule switch actuated by rotation of an encapsulated cluster within a fullerene cage, Chem. Phys. Lett. **552**, 1 (2012).

[4] P. A. Heiney, J. E. Fischer, A. R. McGhie, W. J. Romanow, A. M. Denenstein, J. P. McCauley Jr., A. B. Smith, and D. E. Cox, Orientational ordering transition in solid C_{60}, Phys. Rev. Lett. **66**, 2911 (1991).

[5] N. Ishikawa, M. Sugita, T. Ishikawa, S. Y. Koshihara, and Y. Kaizu, Mononuclear lanthanide complexes with a long magnetization relaxation time at high temperatures: A new category of magnets at the single-molecular level, J. Phys. Chem. B **108**, 11265 (2004).

[6] J. Dreiser, R. Westerström, Y. Zhang, A. A. Popov, L. Dunsch, K. Krämer, S. Liu, S. Decurtins, and T. Greber, The metallofullerene Field-induced single-ion magnet $HoSc_2N@C_{80}$, Chem. Eur. J. **20**, 13536 (2014).

[7] F. Donati, S. Rusponi, S. Stepanow, C. Wäckerlin, A. Singha, L. Persichetti, R. Baltic, K. Diller, F. Patthey, E. Fernandes, J. Dreiser, Ž. Šljivančanin, K. Kummer, C. Nistor, P. Gambardella, and H. Brune, Magnetic remanence in single atoms, Science **352**, 318 (2016).

[8] F. D. Natterer, K. Yang, W. Paul, P. Willke, T. Choi, T. Greber, A. J. Heinrich, and C. P. Lutz, Reading and writing single-atom magnets, Nature (London) **543**, 226 (2017).

[9] R. Westerström, J. Dreiser, C. Piamonteze, M. Muntwiler, S. Weyeneth, H. Brune, S. Rusponi, F. Nolting, A. Popov, S. Yang, L. Dunsch, and T. Greber, An endohedral single-molecule magnet with long relaxation times: $DySc_2N@C_{80}$, J. Am. Chem. Soc. **134**, 9840 (2012).

[10] R. Westerström, J. Dreiser, C. Piamonteze, M. Muntwiler, S. Weyeneth, K. Krämer, S.-X. Liu, S. Decurtins, A. Popov, S. Yang, L. Dunsch, and T. Greber, Tunneling, remanence, and frustration in dysprosium-based endohedral single-molecule magnets, Phys. Rev. B **89**, 060406 (2014).

[11] F. Liu, C.-L. Gao, Q. Deng, X. Zhu, A. Kostanyan, R. Westerström, S. Wang, Y.-Z. Tan, J. Tao, S.-Y. Xie, A. A. Popov, T. Greber, and S. Yang, Triangular monometallic cyanide cluster entrapped in carbon cage with geometry-dependent molecular magnetism, J. Am. Chem. Soc. **138**, 14764 (2016).

[12] F. L. Pratt, E. Micotti, P. Carretta, A. Lascialfari, P. Arosio, T. Lancaster, S. J. Blundell, and A. K. Powell, Dipolar ordering in a molecular nanomagnet detected using muon spin relaxation, Phys. Rev. B **89**, 144420 (2014).

[13] J. Zhang and H. Dorn, NMR studies of the dynamic motion of encapsulated ions and clusters in fullerene cages: A wheel within a wheel, Fullerenes, Nanotubes, Carbon Nanostructures **22**, 35 (2014).

[14] T. Heine, K. Vietze, and G. Seifert, ^{13}C NMR fingerprint characterizes long time-scale structure of $Sc_3N@C_{80}$ endohedral fullerene, Magn. Reson. Chem. **42**, S199 (2004).

[15] J. Dreiser, K. S. Pedersen, C. Piamonteze, S. Rusponi, Z. Salman, M. E. Ali, M. Schau-Magnussen, C. A. Thuesen, S. Piligkos, H. Weihe, H. Mutka, O. Waldmann, P. Oppeneer, J. Bendix, F. Nolting, and H. Brune, Direct observation of a ferri-to-ferromagnetic transition in a fluoride-bridged 3d – 4f molecular cluster, Chem. Sci. **3**, 1024 (2012).

[16] R. Stania, Ph.D. thesis, Universität Zürich, 2016.

[17] W. Fu, X. Wang, H. Azuremendi, J. Zhang, and H. C. Dorn, ^{14}N and ^{45}Sc NMR study of trimetallic nitride cluster $(M_3N)^{6+}$ dynamics inside a icosahedral C_{80} cage, Chem. Commun. (Cambridge) **47**, 3858 (2011).

[18] C. T. Campbell, L. Árnadóttir, and J. R. V. Sellers, Kinetic prefactors of reactions on solid surfaces, Z. Phys. Chem. (Muenchen, Ger.) **227**, 1435 (2013).

[19] A. J. Gellman and K. R. Paserba, Kinetics and mechanism of oligomer desorption from surfaces: *n*-Alkanes on graphite, J. Phys. Chem. B **106**, 13231 (2002).

[20] K. R. Paserba and A. J. Gellman, Effects of conformational isomerism on the desorption kinetics of *n*-alkanes from graphite, J. Chem. Phys. **115**, 6737 (2001).